

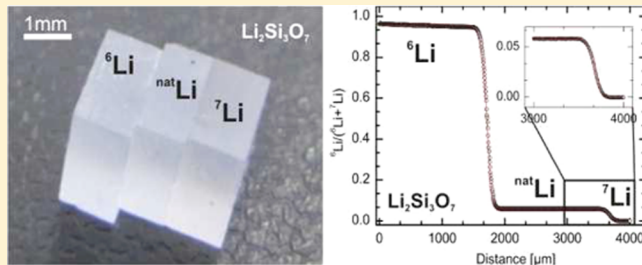
# Li Diffusion and the Effect of Local Structure on Li Mobility in Li<sub>2</sub>O–SiO<sub>2</sub> Glasses

Ute Bauer,<sup>\*,†,‡</sup> Anna-Maria Welsch,<sup>\*,†,‡</sup> Harald Behrens,<sup>†,‡</sup> Johanna Rahn,<sup>§</sup> Harald Schmidt,<sup>‡,§</sup> and Ingo Horn<sup>†</sup>

<sup>†</sup>Institut für Mineralogie und <sup>‡</sup>ZFM - Zentrum für Festkörperchemie und Neue Materialien, Leibniz Universität Hannover, Hannover, Germany

<sup>§</sup>Institut für Metallurgie, Technische Universität Clausthal, Clausthal-Zellerfeld, Germany

**ABSTRACT:** Aimed to improve the understanding of lithium migration mechanisms in ion conductors, this study focuses on Li dynamics in binary Li silicate glasses. Isotope exchange experiments and conductivity measurements were carried out to determine self-diffusion coefficients and activation energies for Li migration in Li<sub>2</sub>Si<sub>3</sub>O<sub>7</sub> and Li<sub>2</sub>Si<sub>6</sub>O<sub>13</sub> glasses. Samples of identical composition but different isotope content were combined for diffusion experiments in couples or triples. Diffusion profiles developed between 511 and 664 K were analyzed by femtosecond laser ablation combined with multiple collector inductively coupled plasma mass spectrometry (fs LA-MC-ICP-MS) and secondary ion mass spectrometry (SIMS). Analyses of diffusion profiles and comparison of diffusion data reveal that the isotope effect of lithium diffusion in silicate glasses is rather small, consistent with classical diffusion behavior. Ionic conductivity of glasses was measured between 312 and 675 K. The experimentally obtained self-diffusion coefficient,  $D_{IE}$ , and ionic diffusion coefficient,  $D_o$ , derived from specific DC conductivity provided information about correlation effects during Li diffusion. The  $D_{IE}/D_o$  is higher for the trisilicate ( $0.27 \pm 0.05$ ) than that for the hexasilicate ( $0.17 \pm 0.02$ ), implying that increasing silica content reduces the efficiency of Li jumps in terms of long-range movement. This trend can be rationalized by structural concepts based on nuclear magnetic resonance (NMR) and Raman spectroscopy as well as molecular dynamic simulations, that is, lithium is percolating in low-dimensional, alkali-rich regions separated by a silica-rich matrix.



## 1. INTRODUCTION

Li-bearing glasses are of interest for various technical applications such as ion conductors or heating devices. Experimental studies on self-diffusion of lithium in glasses are rare.<sup>1–3</sup> The short half-lives of the radioactive Li isotopes (e.g.,  $t_{1/2}(^6\text{Li}) = 0.84$  s;  $t_{1/2}(^9\text{Li}) = 0.18$  s; and  $t_{1/2}(^{11}\text{Li}) = 0.087$  s<sup>4</sup>) prevent the application of classical radioactive tracer methods. Thus, only stable <sup>6</sup>Li and <sup>7</sup>Li isotopes can be utilized in studies of Li dynamics. Assuming classical diffusion behavior, an about 8% higher diffusivity would be expected for <sup>6</sup>Li than for <sup>7</sup>Li due to the mass ratio. Results of Li isotope diffusion studies on lithium silicate glasses by Beier and Frischat<sup>3</sup> are consistent with this expectation. However, pulse field gradient nuclear magnetic resonance (NMR) experiments of Feinauer et al.<sup>5,6</sup> give evidence for even ~25% higher diffusivities of <sup>6</sup>Li in metallic lithium melt. These findings were rationalized in terms of a quantum mechanical theory of diffusion by Omini.<sup>7,8</sup> The crucial question is whether these discrepancies can be attributed to the nature of lithium bonding.

Binary Li silicate glasses where lithium is the only mobile species within a relatively static silicate network are especially suitable as a model system for studying the characteristics of lithium dynamics in disordered ionic materials. In their pioneering work, Beier and Frischat<sup>1–3</sup> have investigated self-

diffusion of lithium in silicate glasses via isotope exchange with lithium nitrate melts followed by mass spectroscopic analyses. Recent advancements in isotope analytics utilizing femtosecond laser ablation combined with multiple collector inductively coupled plasma mass spectrometry (fs LA-MC-ICP-MS) allow measurements of diffusion profiles with significantly higher precision than achievable previously.<sup>9–12</sup> Thus, more detailed information about the diffusivities of lithium isotopes can be extracted from profile analysis.

The present paper is aimed to improve the understanding of the dynamics of lithium in silicate glasses. For doing so, we have studied ionic conductivity and self-diffusion of lithium in Li trisilicate (Li<sub>2</sub>Si<sub>3</sub>O<sub>7</sub>) and Li hexasilicate (Li<sub>2</sub>Si<sub>6</sub>O<sub>13</sub>) glass. The difference in silica content is expected to have a large impact on migration of lithium in these materials. Structural investigations on silica-rich lithium silicate glasses give strong evidence for nonstatistical distribution of lithium in the network.<sup>13–15</sup> Combining results from NMR experiments and molecular dynamic simulations (MDS), Voigt et al.<sup>13</sup> concluded that lithium is concentrated in nanosized low-

Received: September 3, 2013

Revised: November 6, 2013

Published: November 6, 2013

dimensional domains in these structures. In situ measurements by quasielastic neutron scattering indicate that clustering in alkali silicates occurs already in the melt.<sup>16</sup> A pronounced tendency toward nanophase segregation of such glasses was observed upon slow cooling or annealing near the glass transition.<sup>17</sup>

Formation of channels for fast ion diffusion was inferred for lithium, sodium, and potassium disilicate melts by Kargl et al.<sup>16</sup> For systems in which the modifier cations are concentrated in regions and coordinated primarily by NBOs, Greaves and co-workers<sup>18–20</sup> have proposed the modified random network (MRN) model. This model is supported in general terms by structural investigations and simulations as well as studies on the dynamics of alkalis. However, in detail, the MRN model may be oversimplified. <sup>17</sup>O NMR studies of Lee and Stebbins<sup>21</sup> show that both nonbridging oxygens (NBOs) and bridging oxygens (BOs) form the coordination polyhedron of Na in sodium silicate glasses, consistent with the results of Voigt et al.<sup>13</sup> for Li in lithium silicate glasses. As a consequence, alkali cations are not as strictly localized in certain regions of the glass as suggested by the MRN model.

The combination of electrical conductivity data and precisely measured self-diffusivities of Li gives new insight into the dynamics of Li in lithium silicate glasses, that is, correlation factors for Li jumps can be derived. These data will be discussed in the frame of ionic conductivity models for disordered materials. Comparison with recently published data for LiAlSi<sub>2</sub>O<sub>6</sub> allows evaluation of the influence of NBO and [AlO<sub>4</sub>]<sup>-</sup> units on the migration mechanisms of lithium in silicate glasses.<sup>12</sup>

## 2. MATERIAL AND SAMPLE PREPARATION

Li trisilicate (Li<sub>2</sub>Si<sub>3</sub>O<sub>7</sub>) and Li hexasilicate (Li<sub>2</sub>Si<sub>6</sub>O<sub>13</sub>) glasses with different isotopic compositions were prepared by melting stoichiometric powder mixtures of high-purity SiO<sub>2</sub> and Li<sub>2</sub>CO<sub>3</sub>. The specific Li isotope content of glasses was adjusted using lithium carbonate either with the natural isotopic composition (92.58% <sup>7</sup>Li, 7.42% <sup>6</sup>Li) or enriched to either 99.94% <sup>7</sup>Li or 94% <sup>6</sup>Li for essentially monoisotopic Li silicate glasses (Li-enriched materials from Eurisotope). Improved glass homogeneity was achieved by repeating the melting process at 1773 K for 2 h in a covered Pt crucible.

The tendency of binary Li silicate glass toward phase separation has been observed in the past,<sup>1,2,17,22</sup> in particular, for glasses with Li<sub>2</sub>O content between 10 and 24 mol %. Such glasses were typically translucent after cooling due to formation of nanosized Li<sub>2</sub>O-rich droplets surrounded by a SiO<sub>2</sub>-rich matrix. For glasses with <33 mol % Li<sub>2</sub>O, on the basis of phase equilibria considerations,<sup>23,24</sup> Vogel<sup>17</sup> concluded that the Li-rich domains are close to Li<sub>2</sub>Si<sub>2</sub>O<sub>5</sub> stoichiometry. In a glass composed of 27 mol % Li<sub>2</sub>O and 73 mol % SiO<sub>2</sub> (close to lithium trisilicate), Vogel observed that the Li<sub>2</sub>O-rich droplet phases show an average diameter of ~800 Å,<sup>17</sup> inducing slight opacity in the otherwise transparent material. This was taken as an indication of the phase separation. To minimize the risk of phase separation during synthesis of our glasses, the melt was poured onto a brass plate to cool below the glass transition temperature,  $T_g$ , within seconds (cooling rate > 200 K/s). The produced glasses are optically clear and completely transparent and show no indication for microscale phase separation or incipient crystallization (Figure 1). All samples remained unchanged during experimental cycles at high temperatures.

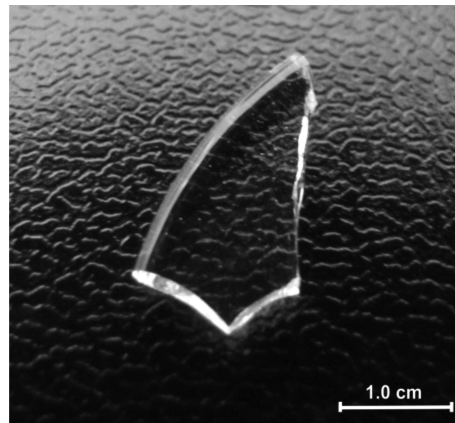


**Figure 1.** <sup>nat</sup>Li<sub>2</sub>Si<sub>3</sub>O<sub>7</sub> glass after rapid-quench shows no visible indications of crystallization or phase separation. Other glasses are of similar quality.

Electron microprobe analysis (EMPA) was used to quantify the silica content and attest that no additional alkali cations were present. Typically, 3–5 analyses were performed across the surface of each glass sample using a Cameca SX-100 microprobe. Measurement conditions included a beam current of 15 nA, an acceleration voltage of 15 kV, a beam size of 5 μm, and counting times of 10–20 s. The programmed matrix correction “PAP” according to Pouchou and Pichoir<sup>25</sup> was used to correct the measured SiO<sub>2</sub> content. EMPA showed that the other alkalis, other possible chemical impurities, were below the detection limit (Table 1). The content of lithium was analyzed by the inductively coupled plasma optic emission spectroscopy (ICP-OES, 715-ES VARIAN). The dissolution of the sample material each with ~100 mg was obtained with microwave digestion using 4 mL of H<sub>3</sub>PO<sub>4</sub>, 3 mL of HNO<sub>3</sub>, and 1 mL of HF. The contents of Li<sub>2</sub>O and SiO<sub>2</sub> are given in Table 1.

Each Li silicate glass was divided in two halves; one-half was used as received, and the second half was annealed near the glass transition temperature  $T_g$  to release internal stresses. The comparison of experiments on both glasses provides some insight into the influence of thermal history on lithium dynamics. For relaxation, selected portions of Li<sub>2</sub>Si<sub>3</sub>O<sub>7</sub> and Li<sub>2</sub>Si<sub>6</sub>O<sub>13</sub> glasses were heated to ~730 K and subsequently cooled at a rate of ~5 K/min to ambient temperature.

The  $T_g$ 's of relaxed glasses were determined by differential thermal analysis (DTA, Setaram Setsys Evolution 1750, heating rate of 5 K/min) as 730 K for the Li<sub>2</sub>Si<sub>3</sub>O<sub>7</sub> glass and 728 K for the Li<sub>2</sub>Si<sub>6</sub>O<sub>13</sub> glass with a precision of ±2 K (Table 1). These values are slightly lower than those reported by Voigt et al.,<sup>13</sup> which is potentially caused by faster quenching in their study. The reliability of the DTA measurement was confirmed using the DGG (German Society of Glass) standard glass I. Measured values of 812.3 K compare to the certified glass transition temperature of (810.5 ± 1.5) K.<sup>26</sup>

Out of each individual synthesized glass, 4 × 4 mm glass plates were prepared for the diffusion couple experiments and impedance measurements. To circumvent the hygroscopic nature of Li silicates, the cutting and polishing had to be performed without exposure to water. For impedance measurements, the quadratic glass plates with a thickness between 1 and 2 mm were only roughly polished, which improved the adhesion of the electrodes during measurement cycles at high temperatures. The standard electrode was of circular shape and made of Ag lacquer (a product by Co. Dr. Ropertz-GmbH)

Table 1. Sample Characterization<sup>a</sup>

sample	theor. NBO/T <sup>b</sup>	Li <sub>2</sub> O <sup>c</sup> [mol %]	SiO <sub>2</sub> <sup>d</sup> [mol %]	deriv. NBO/T	T <sub>g</sub> <sup>e</sup> [K]	ρ <sup>f</sup> [g/cm <sup>3</sup> ]
<sup>nat</sup> Li <sub>2</sub> Si <sub>3</sub> O <sub>7</sub>	0.67	23.33 (0.66)	76.67 (1.09)	0.61	730	2.303 (0.002)
<sup>7</sup> Li <sub>2</sub> Si <sub>3</sub> O <sub>7</sub>		24.04 (0.27)	75.96 (0.62)	0.63		2.305 (0.003)
<sup>6</sup> Li <sub>2</sub> Si <sub>3</sub> O <sub>7</sub>		20.64 (0.66)	79.36 (0.92)	0.57		2.286 (0.003)
<sup>nat</sup> Li <sub>2</sub> Si <sub>6</sub> O <sub>13</sub>	0.33	13.95 (0.37)	86.05 (1.04)	0.33	728	2.243 (0.004)
<sup>7</sup> Li <sub>2</sub> Si <sub>6</sub> O <sub>13</sub>		13.90 (0.04)	86.10 (1.39)	0.32		2.250 (0.005)
<sup>6</sup> Li <sub>2</sub> Si <sub>6</sub> O <sub>13</sub>		13.33 (0.16)	86.67 (0.59)	0.34		2.251 (0.005)

<sup>a</sup>EMPA and ICP-OES chemical composition analyses of Li trisilicate and hexasilicate glasses are normalized to 100 mol %. <sup>b</sup>NBO/T: nonbridging oxygens per tetrahedral cation. <sup>c</sup>Li<sub>2</sub>O contents each based on three individual measurements with ICP-OES. <sup>d</sup>SiO<sub>2</sub> content measured using EMPA; each value is based on five individual measurements. Na<sub>2</sub>O and K<sub>2</sub>O contents determined with EMPA were below the detection limits of 1254 and 919 ppm, respectively. <sup>e</sup>T<sub>g</sub> values were determined using digital thermogravimetric analyses (see text for details). <sup>f</sup>The density was determined using the buoyancy method, that is, by measuring the weight of the sample in air and ethanol.

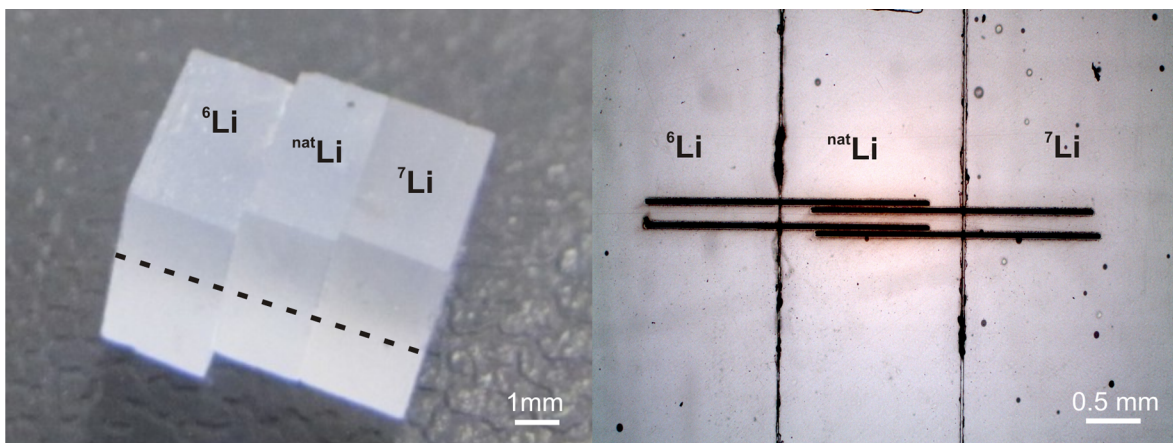


Figure 2. (a) Setup of a diffusion triple. (b) Polished section perpendicular to the interfaces cut roughly in the center of the triple. Lines originate from laser ablation transects crossing the interfaces. Two profiles were measured to check for reproducibility.

with a circular Pt foil mounted on top of the Ag lacquer on each side to produce more regular contact areas of the electrodes. Effective electrode diameters varied between 2.0 and 3.0 mm, resulting in cell constants (electrode area divided by section thickness) between 0.0031 and 0.0038 m.

For the determination of self-diffusion coefficients, glass plates with different Li isotopy were combined into diffusion couples and triples, as shown in Figure 2a.

The diffusion couples combined two glass plates enriched with <sup>6</sup>Li or <sup>7</sup>Li. The triples comprised a combination of two classical diffusion couples. The outer glass plates were enriched in <sup>6</sup>Li and <sup>7</sup>Li, and the middle part was of natural Li isotopic composition. The triple setup enabled the direct comparison of Li mobility in <sup>6</sup>Li-rich and <sup>7</sup>Li-rich glasses. The contact between the glass plates was improved using a thin layer of LiNO<sub>3</sub>, which facilitates the transition of lithium between the glass plates. LiNO<sub>3</sub> with natural isotopic composition was used in the case of diffusion triples, and <sup>6</sup>LiNO<sub>3</sub> was used in the case of diffusion couples. Melting of dry LiNO<sub>3</sub> requires a temperature of 533 K.<sup>4</sup> In order to reduce the melting temperature and avoid any heating-related changes, LiNO<sub>3</sub>·3H<sub>2</sub>O crystals were used as they melt at 303 K and release H<sub>2</sub>O upon further heating. Such crystals can be simply produced by slow evaporation of aqueous LiNO<sub>3</sub> solution. As described in Welsch et al.,<sup>12</sup> a small LiNO<sub>3</sub>·3H<sub>2</sub>O crystal (<1 mg) was placed between the halves of the couple and melted using a hair dryer before the couples were fixed and compressed tightly together in order to generate a film as thin as possible.

### 3. EXPERIMENTS AND ANALYTICAL METHODS

**3.1. Impedance Spectroscopy.** The impedance measurements were conducted in a tube furnace Nabertherm R50/500/13/P330, 1.8 kW with two K-type thermocouples (Ni-Cr<sub>10</sub>Ni<sub>90</sub>) at different positions in close proximity to the sample. This instrumental setup exhibits excellent temperature stability at the center of the furnace (<1 K/cm). Before the measurements, the spectrometer was calibrated using a short-circuit arrangement and a certified 100 Ω resistance. The glass plates were placed in a ceramic sample holder between two Pt<sub>90</sub>Rh<sub>10</sub> cone electrodes, whereby the electrode cones must coincide exactly with the glass plate electrodes. The sample assembly was clamped between the electrodes, securing good sample-electrode connection during the measurement. Electrical conductivity spectra were recorded during the heating sequence, within the 30 min dwell at the maximum temperature, and during the cooling sequence using a Novocontrol Alpha AN impedance analyzer with a four terminal configuration. To avoid changes in the material properties, temperatures were restricted to 649 K for Li<sub>2</sub>Si<sub>3</sub>O<sub>7</sub> and 673 K for Li<sub>2</sub>Si<sub>6</sub>O<sub>13</sub> samples, that is, far below the respective T<sub>g</sub>. The temperature was logged during the whole duration of impedance measurement with 2 s time intervals. Impedance spectra were collected in the frequency range between 0.1 and 10<sup>6</sup> Hz at each selected temperature within 700 s intervals.

**3.2. Isotope Exchange Experiments.** The diffusion experiments were performed in a tube furnace Nabertherm R50/500/13/P330, using the same ceramic sample holder as

that described above for the impedance measurements. In order to reduce the contribution of heating to the isotopic exchange profile, the sample holder was inserted in the preheated furnace. After the experiment, the holder was taken out of the furnace and cooled down to ambient temperature. Typically, heating and cooling times are  $\sim 14$  min up to 673 K and 8 min down to 373 K. The diffusion experiments for  $\text{Li}_2\text{Si}_3\text{O}_7$  samples were conducted in a temperature range between 511 and 664 K, and for the  $\text{Li}_2\text{Si}_6\text{O}_{13}$  samples, they were conducted between 553 and 683 K. Two K-type thermocouples recorded the temperature during the whole experiment in time intervals of 2 s. The effective time ( $t_{\text{eff}}$ ) of the sample exposure at the target temperature ( $T_{\text{eff}}$ ) was calculated as

$$t_{\text{eff}} = \int \exp\left(\frac{-E_{\text{a,DC}}}{R} \cdot \left(\frac{1}{T(t)} - \frac{1}{T_{\text{eff}}}\right)\right) dt \quad (1)$$

where  $E_{\text{a,DC}}$  is the activation energy (based on conductivity measurements; Table 2),  $R$  is the universal gas constant, and  $T(t)$  is the average temperature in the time interval  $dt$ .

**Table 2. Arrhenius Parameters for Ionic Conduction in  $\text{Li}_2\text{Si}_3\text{O}_7$  and  $\text{Li}_2\text{Si}_6\text{O}_{13}$  Glasses<sup>a</sup>**

sample	$T_{\text{range}}$ [K]	$\log A_0$ [ $A_0$ in $\text{S K m}^{-1}$ ]	$E_{\text{a,DC}}$ [kJ/mol]	fit SD
<sup>nat</sup> $\text{Li}_2\text{Si}_3\text{O}_7$	312–671	$7.51 \pm 0.03$	$68.3 \pm 0.01$	0.04
<sup>nat</sup> $\text{Li}_2\text{Si}_6\text{O}_{13}$	318–611	$7.52 \pm 0.02$	$72.4 \pm 0.01$	0.01
<sup>6</sup> $\text{Li}_2\text{Si}_6\text{O}_{13}$	372–666	$7.29 \pm 0.02$	$69.9 \pm 0.01$	0.01
<sup>7</sup> $\text{Li}_2\text{Si}_6\text{O}_{13}$	330–675	$7.11 \pm 0.03$	$68.0 \pm 0.01$	0.03

<sup>a</sup>Quoted errors refer only to the regression. Fit SD is the standard deviation between experimental data and fit results.

Optical inspection of the samples after the experimental run showed no significant changes. Directly following the diffusion experiments, the samples were embedded in epoxy resin (Araldite) and cut in half, perpendicular to the contact plane. The exposed surface was polished for mass spectroscopic measurements.

**3.3. Profile Measurements.** The analyses of the diffusion profiles were performed using fs LA-MC-ICP-MS. In comparison to nanosecond LA systems, internal isotopic fractionation processes can be highly reduced or even avoided by fs laser pulses.<sup>9,10</sup> The deep-UV femtosecond laser system used in this experimental setting is based on a Spectra Physics Solstice Ti–sapphire regenerative amplifier system, comprising a tunable Ti–sapphire femtosecond seed source pumped by a 5 W continuous wave Nd:YLF laser that is internally frequency-doubled to produce 532 nm, a regenerative amplifier pumped by a 15 W internally doubled Nd:YLF, and a pulse stretcher and compressor setup. The output wavelength was set to 775 nm, which generates a beam with a wavelength of 194 nm in the fourth harmonic. Lithium contents were measured with a Thermo Finnigan Neptune multiple collectors ICP-MS using Faraday cups for detection. The ablation cell with a size of  $\sim 35$   $\text{cm}^3$  was provided with inlets for the carrier gas helium with a flow rate of 0.7 L/min, which was mixed before entering the ICP with 0.8 L/min of argon to obtain maximum sensitivity.<sup>10</sup> The pulse width is estimated to be better than 200 fs in the deep-UV, and the repetition rate was 5 Hz. The detailed description of the experimental setup has been presented in refs 10 and 11.

The sample stage with an accuracy of positioning better than  $\pm 1 \mu\text{m}$  enables line scans perpendicular to the contact plane of the glass halves in a continuous mode. In order to reach a high number of data points at the interface, the scan speed was chosen individually for each diffusion profile and varied between 1 and 10  $\mu\text{m/s}$ . The diameter of the ablation hole was typically 30  $\mu\text{m}$ . Considering the mass spectrometric integration time of 1 s and the corresponding scan speed, the effective spatial resolution of the laser beam was 30–40  $\mu\text{m}$ . For technical reasons, the diffusion profiles exceeding 1000  $\mu\text{m}$  had to be divided into two overlapping regions, as presented in Figure 2b, and each part was processed individually. To check the reproducibility, the profiles were measured twice (Figure 2b). The recorded raw intensities were background-corrected using the background data derived from the gas blank, which was measured prior to the ablation interval. To eliminate variability of the signal due to differences in material transport rates from the ablation cell to the ICP, the intensity of the <sup>6</sup>Li signal was normalized to the total Li content, that is, <sup>6</sup>Li/(<sup>6</sup>Li + <sup>7</sup>Li). On the basis of the repeated analyses and calculations, the diffusion coefficients can be defined with the certainty of  $\sim 93\%$ .

SIMS analyses were conducted for comparison to the laser ablation measurements. Analyses were performed using a CAMECA IMS-3F/4F instrument with an O<sup>-</sup> primary ion beam (15 keV and 5–20 nA).<sup>27</sup> The primary beam was focused on the sample, and measurements were performed in the line scan mode by moving the sample parallel to the sample interface. Short depth profiles at each measuring point allowed the exact determination of the ratio of the two Li isotopes. The analyses of the sputtered material (from an area of about  $50 \times 50 \mu\text{m}^2$ ) were performed using a double-focusing mass spectrometer combined with an electron multiplier. Due to the identical ionization energies of <sup>6</sup>Li and <sup>7</sup>Li isotopes, the counting rates can be directly used to calculate the relative isotope fractions along the line scan.

## 4. RESULTS

**4.1. Conductivity.** In order to determine the specific DC conductivity,  $\sigma_{\text{DC}}$ , the measured impedance was corrected by dividing through the cell constant. Thus-derived conductivity spectra are plotted as a function of frequency in Figure 3a.

The frequency-independent conductivity plateau defines the DC conductivity. From this low-frequency plateau,  $\sigma_{\text{DC}}$  values for each temperature are determined approximately in the center of each plateau. The DC conductivity for the measured Li silicate glasses can be well-described in the tested temperature range by the Arrhenius relation

$$\sigma_{\text{DC}} T = A_0 \cdot \exp\left(\frac{-E_{\text{a,DC}}}{RT}\right) \quad (2)$$

where  $A_0$  is the pre-exponential factor and  $E_{\text{a,DC}}$  is the activation energy for ionic conduction. The Arrhenius parameters for the glasses are listed in Table 2. Conductivity studies of  $\text{LiAlSi}_2\text{O}_6$  glasses with different origin and different electrode materials<sup>12</sup> demonstrate the accuracy of the experimental method to be within  $\pm 10\%$ .

The results of conductivity measurements show only slightly higher conductivity of Li trisilicate in comparison to Li hexasilicate glass (Figure 3b). Hence, the small variations in the Li/Si ratio of the different synthesized Li trisilicate glasses (Table 1) is expected to have a minor effect on the transport of lithium in these materials. In the case of the Li hexasilicate

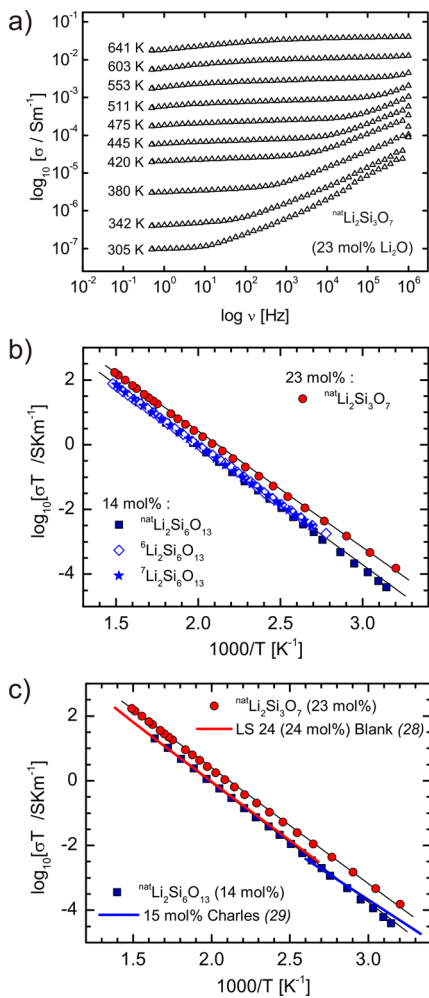


**Figure 3.** (a) Conductivity spectra of <sup>nat</sup>Li<sub>2</sub>Si<sub>3</sub>O<sub>7</sub> glass. (b) Arrhenius plot for lithium trisilicate and hexasilicate samples. Note the absence of an isotope effect in the case of the hexasilicate. (c) Comparison of Li<sub>2</sub>Si<sub>3</sub>O<sub>7</sub> and Li<sub>2</sub>Si<sub>6</sub>O<sub>13</sub> samples with a natural isotope composition with literature data. The mol % refers to the Li<sub>2</sub>O content of the glasses. Error bars are smaller than the symbols.

glass, no effect of different isotope ratios on conductivity was observed (Figure 3b). In comparison to conductivity data of Blank,<sup>28</sup> our results show a slightly higher conductivity in the case of the Li trisilicate, whereas the data of Charles<sup>29</sup> are in

very good agreement with our data determined for the Li hexasilicate (Figure 3c).

**4.2. Diffusivity.** Under the assumption that the diffusion coefficients are concentration-independent and that the profiles do not reach the end faces of the samples, the solution for Fick's second law<sup>30</sup> for one-dimensional diffusion between semi-infinite media is given as

$$\frac{(c - c_0)}{(c_1 - c_0)} = \frac{1}{2} \cdot \left( 1 - \operatorname{erf} \left( \frac{x - a}{\sqrt{4D_{IE}t}} \right) \right) \quad (3)$$

where  $c$  is the concentration at distance  $x$ ,  $c_0$  and  $c_1$  are the initial concentrations in each segment of the diffusion couple,  $a$  corresponds to the inflection point of the profiles,  $D_{IE}$  is the diffusion coefficient determined from isotope exchange experiments, and  $t$  is the duration of the diffusion experiment.<sup>31</sup> The prerequisite for using the isotopic ratio <sup>6</sup>Li/(<sup>6</sup>Li + <sup>7</sup>Li) as a concentration variable is a constant lithium content over the whole profile. As can be seen in Table 1, Li<sub>2</sub>O contents at the interface initially differ between 3 and 15%. Because redistribution of lithium in the glasses is limited by oxygen diffusion, which is negligible below the glass transition, the lithium concentration profiles will not change on the time scale of the isotope exchange experiments. No discontinuity of the profiles is observed at the interface of both halves of the couple, which demonstrates that neither small differences in Li/Si of both halves nor the small amount of LiNO<sub>3</sub> between the halves have an influence on the diffusion process.

In order to derive  $D_{IE}$ , the diffusion profiles were fitted using eq 3. In the case of triples, profiles in the two contact zones were evaluated individually. The zero point of the  $x$  axis was arbitrary chosen, and thus, the inflection point on the profile became an adjustable fitting parameter. The collected data are high-symmetry profiles, which are excellently reproduced by the fitting curves (Figure 4), implying that any potential variation in the  $D_{IE}$  with the isotopic ratio is too small to be resolved with the applied analytical techniques.

Thus, the calculated values given in Table 3 can be considered as average self-diffusion coefficients of lithium for the corresponding material and the isotopic range of lithium. No difference in lithium self-diffusivity was observed for relaxed and unrelaxed glasses (Figure 5).

A comparison of self-diffusion coefficients derived from SIMS analyses with fs LA-MC-ICP-MS data is included in Figure 5. It is important to note that in the present case, the spatial resolution of SIMS was lower in comparison with the fs

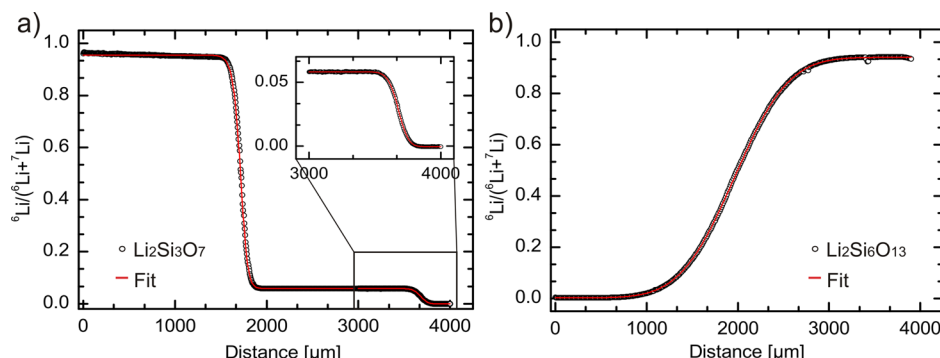


**Figure 4.** Isotope profiles measured with ICP-MS coupled with fs laser ablation. (a) Li<sub>2</sub>Si<sub>3</sub>O<sub>7</sub> diffusion triple after 55 min at 616 K. The half with low <sup>6</sup>Li is enlarged for clarity. (b) Li<sub>2</sub>Si<sub>6</sub>O<sub>13</sub> diffusion couple, annealed at 623 K for 1200 min. The red line represents fitting assuming constant diffusivity.

Table 3. Experimental  $t-T$  Parameters and Diffusion Data along with Literature Data for Comparison<sup>a</sup>

sample	c Li <sub>2</sub> O <sup>b</sup> [mol %]	reference	$T_{\text{eff}}$ [K]	$t_d$ [s]	$t_{\text{eff}}$ [s]	$D_{IE}$ [m <sup>2</sup> /s]	$D_{\sigma}^{d,e}$ [m <sup>2</sup> /s]	$H_R/f$
$\text{Li}_2\text{Si}_6\text{O}_{13}$								
LH-r-1	~14	this study	683	72888	73272	$(1.49 \pm 0.26) \times 10^{-12}$	$(7.67 \pm 0.84) \times 10^{-12}$	$0.19 \pm 0.04$
LH-r-2			623	332691	333366	$(3.94 \pm 0.85) \times 10^{-13}$	$(2.25 \pm 0.28) \times 10^{-12}$	$0.17 \pm 0.04$
LH-r-3- <sup>6</sup> Li			553		777600 <sup>c</sup>	$(6.02 \pm 1.61) \times 10^{-14}$	$(3.83 \pm 0.40) \times 10^{-13}$	$0.15 \pm 0.05$
LH-r-3- <sup>7</sup> Li						$(5.89 \pm 1.58) \times 10^{-14}$		$0.15 \pm 0.04$
LS18	18	1–3		561				
				585		$2.08 \times 10^{-13}$	$5.04 \times 10^{-13}$	0.41
				615		$3.83 \times 10^{-13}$	$9.08 \times 10^{-13}$	0.42
				653		$6.99 \times 10^{-13}$	$1.78 \times 10^{-12}$	0.39
				685		$1.42 \times 10^{-12}$	$3.84 \times 10^{-12}$	0.37
						$2.80 \times 10^{-12}$	$6.88 \times 10^{-12}$	0.41
$\text{Li}_2\text{Si}_3\text{O}_7$								
LT-r-1	~23	this study	593	911	1599	$(4.17 \pm 1.10) \times 10^{-13}$	$(1.37 \pm 0.14) \times 10^{-12}$	$0.30 \pm 0.09$
LT-r-1						$(3.89 \pm 1.03) \times 10^{-13}$		$0.28 \pm 0.08$
LT-r-3			511	89242	89850	$(2.75 \pm 0.98) \times 10^{-14}$	$(1.49 \pm 0.15) \times 10^{-13}$	$0.18 \pm 0.07$
LT-r-3						$(2.48 \pm 0.89) \times 10^{-14}$		$0.17 \pm 0.06$
LT-r-4- <sup>6</sup> Li			616	2491	3315	$(6.88 \pm 1.59) \times 10^{-13}$	$(2.30 \pm 0.24) \times 10^{-12}$	$0.30 \pm 0.08$
LT-r-4- <sup>7</sup> Li						$(6.01 \pm 1.39) \times 10^{-13}$		$0.26 \pm 0.07$
LT-r-6- <sup>6</sup> Li			664	11032	11817	$(1.62 \pm 0.34) \times 10^{-12}$	$(6.05 \pm 0.63) \times 10^{-12}$	$0.27 \pm 0.06$
LT-r-6- <sup>7</sup> Li						$(1.64 \pm 0.35) \times 10^{-12}$		$0.27 \pm 0.06$
LT-u-7- <sup>6</sup> Li			556	81946	82787	$(1.40 \pm 0.40) \times 10^{-13}$	$(5.47 \pm 0.57) \times 10^{-13}$	$0.25 \pm 0.08$
LT-u-7- <sup>7</sup> Li						$(1.35 \pm 0.40) \times 10^{-13}$		$0.26 \pm 0.08$
LT-u-8- <sup>6</sup> Li			664	2849	3711	$(1.92 \pm 0.47) \times 10^{-12}$	$(6.04 \pm 0.63) \times 10^{-12}$	$0.34 \pm 0.09$
LT-u-8- <sup>7</sup> Li						$(2.07 \pm 0.44) \times 10^{-12}$		$0.32 \pm 0.08$
LS25	1,2			709		$4.10 \times 10^{-12}$		$0.4–0.5$
				667		$2.10 \times 10^{-12}$		
				588		$4.80 \times 10^{-13}$		
$\text{Li}_2\text{Si}_2\text{O}_5$								
LS33	25	1–3		557		$2.09 \times 10^{-13}$	$2.48 \times 10^{-13}$	0.84
				585		$5.44 \times 10^{-13}$	$5.12 \times 10^{-13}$	1.06
				638		$1.40 \times 10^{-12}$	$1.70 \times 10^{-12}$	1.00
				667		$2.79 \times 10^{-12}$	$3.04 \times 10^{-12}$	0.92
				705		$6.56 \times 10^{-12}$	$6.05 \times 10^{-12}$	1.08
				723		$9.86 \times 10^{-12}$	$8.21 \times 10^{-12}$	1.20

<sup>a</sup>(LT-r) and (LT-u) denotes relaxed and unrelaxed  $\text{Li}_2\text{Si}_3\text{O}_7$  samples, respectively.  $T_{\text{eff}}$  is the average temperature during the high-temperature dwell, and  $t_{\text{eff}}$  is the effective time at  $T_{\text{eff}}$  calculated by eq 1;  $t_d$  is the time that the sample spends at the maximum  $T_{\text{eff}} \pm 5$  K. <sup>b</sup>The lithium concentration ( $c_{\text{Li}}$ ) for the calculation of  $D_{\sigma}$  is based on the Nernst–Einstein relation (eq 5):  $c_{\text{Li}}^{(\text{nat})}\text{Li}_2\text{Si}_3\text{O}_7 = 20261 \text{ mol/m}^3$ ;  $c_{\text{Li}}^{(\text{nat})}\text{Li}_2\text{Si}_6\text{O}_{13} = 11201 \text{ mol/m}^3$ . <sup>c</sup>The experiment was interrupted twice due to a heating power break, but  $T$  was continuously recorded. <sup>d</sup> $D_{\sigma}$  is calculated from eq 5 using the DC conductivity data from <sup>nat</sup>LT-r.  $H_R/f$  is the correlation factor calculated as the ratio between  $D_{IE}$  and  $D_{\sigma}$ ; see the text for more details. <sup>e</sup>The error calculation for  $D_{\sigma}$  is based on (i) an estimated error of  $\pm 10\%$  for  $\sigma_{DC}$ , as given in Welsch et al.,<sup>12</sup> (ii)  $\pm 3$  K as uncertainties for the temperature measurements, and (iii) uncertainties in density and  $\text{Li}_2\text{O}$  concentration [mol %] used to calculate the concentration of Li ( $c_{\text{Li}}$ ). <sup>f</sup>The error is a rough estimate only because the diffusion experiment was above the temperature range of the conductivity experiments.

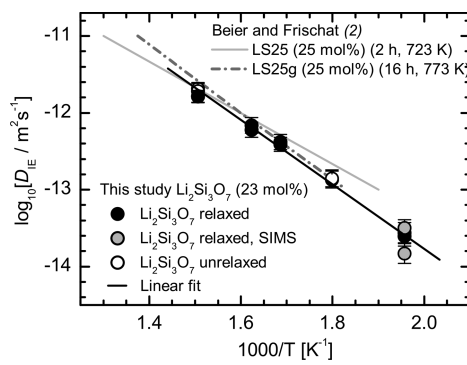


Figure 5. Effect of thermal history on self-diffusion in  $\text{Li}_2\text{Si}_3\text{O}_7$  glass and comparison with results from Beier and Frischat.<sup>2</sup> LS25 and LS25g refer to labels used by Beier and Frischat<sup>2</sup> for glasses with nominal  $\text{Li}_2\text{Si}_3\text{O}_7$  composition. Preannealing conditions in that study are given in parentheses. The mol % refers to the  $\text{Li}_2\text{O}$  content of the glasses. For details, see the text.

LA MC-ICP-MS, resulting in fewer points in the vicinity of the contact between parts of couples/triples. Hence, the diffusivity derived from the SIMS measurements exhibits larger errors. Nevertheless, the agreement with fs LA-MC-ICP-MS data is within 0.2 log units.

## 5. DISCUSSION

**5.1. Isotope Effect.** Significantly higher differences between the diffusivities of <sup>6</sup>Li and <sup>7</sup>Li were observed in metallic melts in comparison with oxide glasses.<sup>5,6</sup> The differences most likely originate from the structure of the materials and the type of lithium bonding. Collective motions in metallic melts result in a pronounced lithium isotope effect.<sup>5,6</sup> In oxide materials, lithium ions are strongly affected by local Coulomb forces, and the migration of lithium is constrained by the potential landscape in the oxide framework.<sup>32,33</sup>

On the basis of deviations from symmetry in experimentally determined diffusion profiles, Beier and Frischat<sup>1</sup> concluded for Si-rich lithium silicate glasses that <sup>6</sup>Li diffusivity is 3–6% faster

than  ${}^7\text{Li}$  diffusivity, with the difference decreasing with temperature. However, as noted by the authors, the observed isotopic trends may be affected by phase separations in the glasses and may not directly represent differences in isotope diffusivities. Despite of these limitations, their study clearly demonstrates that the isotope effect of lithium diffusion in silicate glasses is rather small, consistent with classical diffusion behavior.

Our data presented in Figure 6 are in agreement with these findings. Diffusion coefficients derived for  ${}^6\text{Li}$ -rich and  ${}^7\text{Li}$ -rich

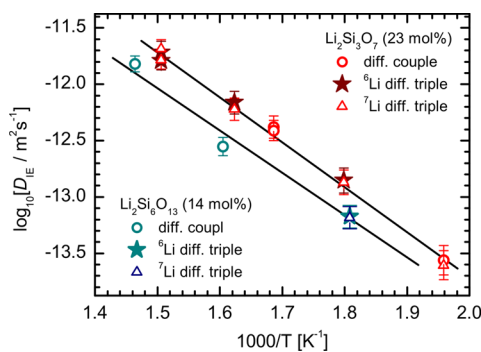


**Figure 6.** Li self-diffusion coefficients determined by isotope exchange experiments ( $D_{\text{Li},\text{IE}}$ ) in  $\text{Li}_2\text{Si}_3\text{O}_7$  and  $\text{Li}_2\text{Si}_6\text{O}_{13}$  glasses.  ${}^6\text{Li}$  and  ${}^7\text{Li}$  designation refers to the predominant isotope in the respective part of a triple.

parts of three of the  $\text{Li}_2\text{Si}_3\text{O}_7$  triples differ only by 1–7% (see Table 3). In the fourth diffusion triple (LT-r-4), a difference of almost 14% was determined, although in that case, the diffusion profile was relatively short ( $\sim 450 \mu\text{m}$ ), increasing the error due to spatial laser resolution.

The  $\text{Li}_2\text{Si}_6\text{O}_{13}$  triple LH-r-3 also yields a very small difference of 2% for lithium self-diffusion in the  ${}^6\text{Li}$ -rich and  ${}^7\text{Li}$ -rich regions.

Because the diffusion coefficient averages over the isotopic range along the profile, the difference between  ${}^6\text{Li}$ -rich and  ${}^7\text{Li}$ -rich parts of the triple is expected to be smaller than the square root of the mass ratio of  ${}^6\text{Li}/{}^7\text{Li}$ . Assuming that the derived diffusivity corresponds to the isotopic ratio at the inflection point of the profile, the difference should be only  $\sim 4\%$ . In conclusion, the available lithium diffusion data for silicate glasses concur with a classical diffusion behavior of lithium, but the exact ratio of  $D({}^6\text{Li})/D({}^7\text{Li})$  cannot be determined by profile analysis.

Considering indistinguishable diffusivities of both lithium isotopes, the data plotted in Figure 6 were used to constrain the temperature dependence of lithium diffusivity for each composition. The derived Arrhenius parameters are listed in Table 4. It is worth noting that the parameters for lithium hexasilicate are based on four profiles only and, hence, may have larger uncertainty than those for lithium trisilicates. On

**Table 4. Arrhenius Parameters for Self-Diffusion in  $\text{Li}_2\text{Si}_3\text{O}_7$  and  $\text{Li}_2\text{Si}_6\text{O}_{13}$  Glasses<sup>a</sup>**

sample	$T_{\text{range}}$ [K]	$\log D_0$ [ $D_0$ in $\text{m}^2/\text{s}$ ]	$E_{\text{a,IE}}$ [kJ/mol]	fit SD
$\text{Li}_2\text{Si}_3\text{O}_7$	551–664	$-5.68 \pm 0.17$	$75.7 \pm 0.09$	0.05
$\text{Li}_2\text{Si}_6\text{O}_{13}$	553–683	$-6.31 \pm 0.62$	$74.7 \pm 0.36$	0.11

<sup>a</sup>Quoted errors refer only to the regression. Fit SD is the standard deviation between experimental data and fit results.

the other hand, the large temperature range covered by the experiments provides confidence in these values.

**5.2. Structure of Lithium Silicate Glasses.** As proven by many previous studies, local structural arrangement in glass and the degree of polymerization within the network have strong impact on cation transport properties.<sup>14,16</sup> Addition of  $\text{Li}_2\text{O}$  to  $\text{SiO}_2$  results in depolymerization of the structure, that is, the excess oxygen breaks  $\text{Si}=\text{O}=\text{Si}$  bonds and NBOs are thus formed. The expected degree of depolymerization in a glass can be expressed as a chemical parameter based on the fraction of NBO per tetrahedrally coordinated cation (NBO/T). The Li trisilicate with NBO/T of  $\sim 0.67$  is significantly more depolymerized than Li hexasilicate, with NBO/T of  $\sim 0.33$ . The number of NBOs per  $\text{SiO}_4$  tetrahedral unit defines the type of  $Q^i$  species,<sup>34,35</sup> that is,  $Q^4$  contains only BO,  $Q^3$  one NBO,  $Q^2$  two NBOs, and so forth. According to NMR studies of Schramm et al.<sup>36</sup> and Voigt,<sup>13</sup> the average abundance is 48–55% of  $Q^4$ , 33–37% of  $Q^3$ , and 6–12% of  $Q^2$  in  $\text{Li}_2\text{Si}_6\text{O}_{13}$  glass, while in  $\text{Li}_2\text{Si}_3\text{O}_7$ , the average distribution is 30–35% of  $Q^4$ , 56–58% of  $Q^3$ , and 7–11% of  $Q^2$ .<sup>36</sup>

$Q$  speciation in the glasses of our study was analyzed by Raman spectroscopy following the procedure developed by Zakaznova-Herzog et al.<sup>37,38</sup> and Malfait et al.<sup>39,40</sup> for alkali and earth-alkali silicate glasses. The mode analyses and assignment given by this approach stand in agreement with the analyses given in earlier Raman studies<sup>34,41,42</sup> as well as the NMR  $Q$  species quantification.<sup>13,36</sup> Furthermore, this approach offers an improved understanding of the vibrational mode origins. The Raman spectra collected for our  $\text{Li}_2\text{Si}_3\text{O}_7$  and  $\text{Li}_2\text{Si}_6\text{O}_{13}$  glasses were background- and temperature-corrected, as given in Welsch et al.,<sup>12</sup> and deconvoluted assuming Gaussian peak shapes for the individual active modes, as shown in Figure 7.

The ratio of integrated intensities of the subpeaks is almost constant for  $Q^4$  and  $Q^2$  when comparing different lithium silicate compositions, while the intensities of the different band systems strongly depend on the silica content. The relative abundance for each of the  $Q$  species was obtained by dividing

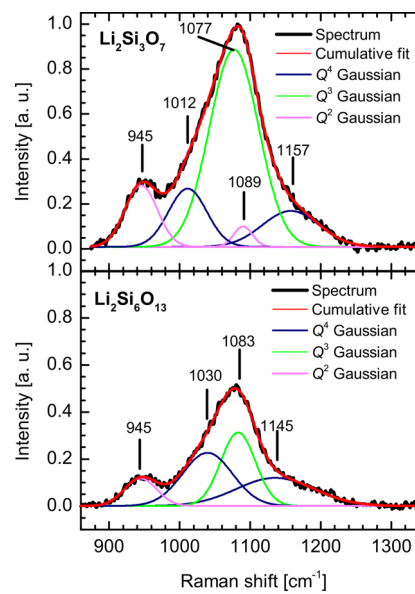


**Figure 7.** High-energy region in the Raman spectra of  $\text{Li}_2\text{Si}_3\text{O}_7$  and  $\text{Li}_2\text{Si}_6\text{O}_{13}$ , deconvoluted into individual Gaussian profiles corresponding to the individual type of  $Q$  species present. The deconvolution followed the model given in Zakaznova-Herzog et al.<sup>37</sup>

the sum of the peak areas belonging to the same  $Q$  species by the overall integrated high-energy area used for quantification. For our  $\text{Li}_2\text{Si}_3\text{O}_7$  glass, the  $Q^4$  species is present with 29%,  $Q^3$  with 57%, and  $Q^2$  with 14%, while the abundance of  $Q^4$  species in  $\text{Li}_2\text{Si}_6\text{O}_{13}$  is 58, that of  $Q^3$  is 31%, and that of  $Q^2$  is 11%. Both data are in good agreement with the published NMR values.<sup>13,36</sup>

The abundance of  $Q^i$  species can be used for defining the degree of depolymerization per  $\text{SiO}_4$  tetrahedron

$$\frac{\text{NBO}}{T} = \frac{\sum_0^i [(4-i) \cdot Q^i]}{\sum (Q^i)} \quad (4)$$

This structurally based definition of NBO/T has to be distinguished from the compositionally based definition (where NBO/T reflects the Li/Si ratio). Both NMR data from literature<sup>13,36</sup> and our Raman-based  $Q$  species quantification indicate an apparently higher degree of depolymerization than that expected by the  $\text{Li}_2\text{O}$  content, that is, NBO/T of 0.72–0.85 for  $\text{Li}_2\text{Si}_3\text{O}_7$  and ~0.50 for  $\text{Li}_2\text{Si}_6\text{O}_{13}$  based on NMR data compared to 0.67 and 0.33, respectively, based on chemical composition. When comparing NMR data for alkali silicate glasses with different alkalis but the same alkali/silica ratio, it appears that the discrepancy between the NBO/T definitions decreases with cation size.<sup>43–47</sup> In contrast to  $\text{Li}_2\text{Si}_3\text{O}_7$ ,  $Q^3$  is the only depolymerized  $Q$  species in  $\text{Na}_2\text{Si}_3\text{O}_7$  and  $\text{K}_2\text{Si}_3\text{O}_7$  glasses with abundances of ~60 and ~63%, respectively,<sup>48,49</sup> corresponding to NBO/T values of 0.60 and 0.63, respectively. Both are in good agreement with the composition-based NBO/T value of 0.67. These observations can be attributed to the high ionic field strength (charge/radius<sup>2</sup>; ionic radii based on Shannon and Prewitt<sup>50</sup>) of Li in comparison with Na and K, that is, Li ( $2.87 \text{ \AA}^{-2}$ ) > Na ( $1.02 \text{ \AA}^{-2}$ ) > K ( $0.52 \text{ \AA}^{-2}$ ), when the coordination numbers (Li (4), Na (4), K (5)) are considered as closest to the experimentally determined values. The coordination number in different binary alkali silicate glasses has been experimentally determined to be between 4 and 5 around K<sup>51</sup> and 3 and 4 around Na atoms,<sup>52</sup> while Li is coordinated by 2–4 oxygens,<sup>14,15,53,54</sup> including not only NBO but also BO. The large ionic field strength of Li induces a change in the character of a neighboring Si toward lower  $Q$  species number. This effect will be particularly pronounced when two or more Li ions are close to a  $Q^4$  species. Hence, the high values obtained by eq 4 indicate the formation of lithium-rich regions in the silicate network.

A separation of Li-rich regions within a Si-rich matrix was observed by different experimental methods<sup>13,15,16,21,53,55–57</sup> as well as theoretical modeling.<sup>13,14,58–60</sup> Analyses of Li–NBO and Li–BO bond lengths and spatial arrangements by NMR,<sup>13,55,56</sup> neutron diffraction,<sup>15,53,54</sup> MDS,<sup>13,14,58–60</sup> and the low coordination number of Li<sup>14,54</sup> strongly point toward elongated channel-like arrangements of the Li-rich regions. Quasielastic neutron scattering results corroborate the formation of cation channels for fast ion diffusion in the static Si matrix as a feature of all alkali binary silicates.<sup>16</sup> Preferential Li cation migration paths can thus be formed between individual interconnected Li-rich regions by cation hopping over the percolation barriers, that is, between the depolymerized  $Q$  species. Li self-diffusion would be strongly influenced by the volume and cation density of such Li-rich regions,<sup>13</sup> the degree of interconnectivity, the constriction of the percolation barriers, as well as the tortuosity of the resulting percolation path. As such, taking into account the low dimensionality of this

nonrandom migration process, some similarities with macroscopic diffusion in porous media can be observed, that is, systems that consist of a network of interconnected pores separated by impermeable regions.<sup>61</sup> It is conceivable to expect the ionic diffusivity to be mainly influenced by the abundance of cation-rich regions and the short-range forward–backward jumps within individual regions. Theoretical models<sup>32,33,59</sup> indicate that the simultaneous jumps of neighboring lithium atoms contribute collectively to the diffusive dynamics, causing local relaxation in the potential landscape and reducing the electronegative potential barrier for subsequent Li jumps on a short time scale.

These structural arrangements in terms of variations in spatial distribution, abundance, size, and connectivity of Li-rich regions are also strongly influenced by the thermal history of the glass,<sup>1,2,22</sup> which may have significant impact on lithium mobility. Hench et al.<sup>22</sup> noticed a significant reduction of conductivity of ~2 orders of magnitude in Li silicate glass with 33 mol %  $\text{Li}_2\text{O}$  after pretreatment of 100 h at 773 K ( $T_g + 40 \text{ K}$ ). Beier and Frischat<sup>1,2</sup> tempered a Li trisilicate sample (LS25: 25 mol %  $\text{Li}_2\text{O}$ ) at 723 K for 2 h and another Li trisilicate glass (LS25g) at 773 K for 16 h and observed that annealing about 40 K above  $T_g$  does not have a drastic impact on self-diffusion, although the activation energy is increased for the tempered sample (LS25: 64.1 kJ/mol; LS25g: 80.9 kJ/mol), as shown in Figure 5. This observation was interpreted in terms of local-scale unmixing and the formation of nanosized  $\text{Li}_2\text{Si}_2\text{O}_5$  seeds through the depletion of the Li content from the glass matrix<sup>1,2</sup> in the case of LS25g, consistent with the observation by Vogel.<sup>17</sup> Thus, the ion transport would be hindered as a consequence of nanoscale phase separation and regions with higher silica content, acting as insulators around Li-rich regions.

Contrary to Hench et al.<sup>22</sup> and Beier and Frischat,<sup>1,2</sup> our samples were not annealed for a long time in the vicinity of  $T_g$ . Self-diffusion data of unrelaxed glasses and glasses held for a few minutes near  $T_g$  before cooling slowly to room temperature (relaxed glasses) exhibited no effect of the thermal pretreatment, Figure 5.

**5.3. Effect of Composition on Lithium Mobility.** Self-diffusivities of lithium in short-term annealed samples of Beier and Frischat<sup>1,2</sup> (LS18, LS25, and LS33, preannealed for 2 h at 723 K) are in very good agreement with our isotope exchange data for lithium trisilicate glass (Figure 8).

The slightly lower Li diffusivity in the hexasilicate glass can be explained by a compositional effect. Figure 9 shows a comparison of lithium diffusivities for lithium silicate glasses based on three different methods (isotope exchange, electrical conductivity, MDS).

Using the specific conductivity  $\sigma_{i,\text{DC}}$ , the ionic diffusivity  $D_{i,\sigma}$  was calculated using the Nernst–Einstein relation

$$D_{i,\sigma} = \frac{RT\sigma_{i,\text{DC}}}{c_i z_i^2 F^2} \quad (5)$$

where  $c_i$  is the concentration of mobile species  $i$ ,  $z_i$  stands for the ionic charge,  $F$  is the Faraday constant,  $R$  equals the universal gas constant, and  $T$  is the absolute temperature. The concentration of lithium (in mol/m<sup>3</sup>) was calculated as

$$c_{\text{Li}} = \frac{2 \cdot \text{mol \% Li}_2\text{O}}{\text{mol \% Li}_2\text{O} \cdot M_{\text{Li}_2\text{O}} + \text{mol \% SiO}_2 \cdot M_{\text{SiO}_2}} \rho \quad (6)$$

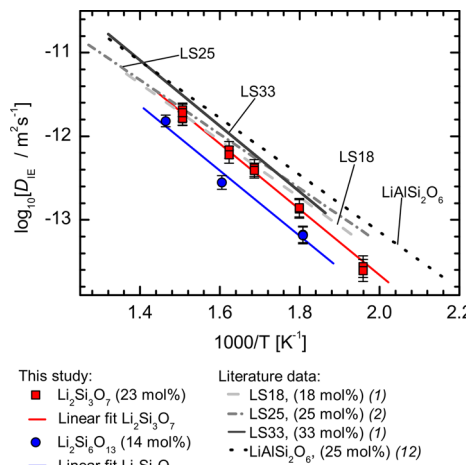


**Figure 8.** Comparison of self-diffusivities based on isotope exchange experiments for lithium in silicate and aluminosilicate glasses. Regression lines are plotted for literature data. Labels of Beier and Frischat correspond to nominal compositions  $\text{Li}_2\text{Si}_6\text{O}_{13}$  (LS18),  $\text{Li}_2\text{Si}_3\text{O}_7$  (LS25), and  $\text{Li}_2\text{Si}_2\text{O}_5$  (LS33). The mol % refers to the  $\text{Li}_2\text{O}$  content of the glasses.

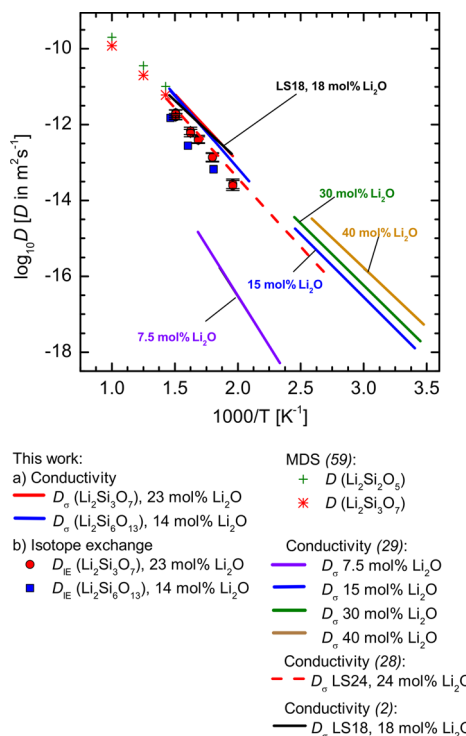


**Figure 9.** Comparison of Li self-diffusivities in lithium silicates determined by isotope exchange experiments in our study with diffusivities based on MDS<sup>59</sup> and calculated by eq 5 using conductivity data from our study and from the literature.<sup>1,28,29</sup>

using mole percent of oxides and the density  $\rho$  of the glass (from Table 1 or from the literature) and the molar mass  $M$  of  $\text{Li}_2\text{O}$  and  $\text{SiO}_2$ .

$D_\sigma$  derived from conductivity measurements of Charles<sup>29</sup> in the low-temperature range are in good agreement with our data at elevated temperatures (Figure 9). In the range of 15–40 mol %  $\text{Li}_2\text{O}$ , the calculated  $D_\sigma$  values rise continuously with increasing  $\text{Li}_2\text{O}$  content. MDS at 700, 800, and 900 K by Habasaki and Hiwatari<sup>59</sup> are consistent with the experimentally

derived diffusion coefficients. Combining the results of the theoretical modeling<sup>59</sup> and experimental data, the lithium diffusivity in glasses with contents between 14 and 33 mol %  $\text{Li}_2\text{O}$  exhibits an almost linear relation on reciprocal temperature over a wide temperature range and small variations with  $\text{Li}_2\text{O}$  content. Interestingly, these compositional effects seem to vanish after thermal treatment. As noticed above, similar lithium diffusivities were found in tempered glasses with 18 and 33 mol %  $\text{Li}_2\text{O}$  by Beier and Frischat.<sup>1,2</sup>

A significant decrease in lithium diffusivity is evident toward low  $\text{Li}_2\text{O}$  content. The high amount of  $\text{SiO}_2$ -rich matrix causes a larger distancing between the isolated Li-rich regions. This reduced interconnectivity between Li-rich areas results in a higher activation energy and a pronounced decrease in long-range Li diffusion. These observations indicate a change from better interconnected to more isolated Li-rich regions in the range from 14 to 7.5 mol %  $\text{Li}_2\text{O}$ .

**5.4. Correlation Effects on Lithium Migration.** The specific role of Li clustering in cation migration in  $\text{Li}_2\text{Si}_3\text{O}_7$  and  $\text{Li}_2\text{Si}_6\text{O}_{13}$  is reflected in the differences between the ionic and self-diffusivities, as given in Figure 10a.

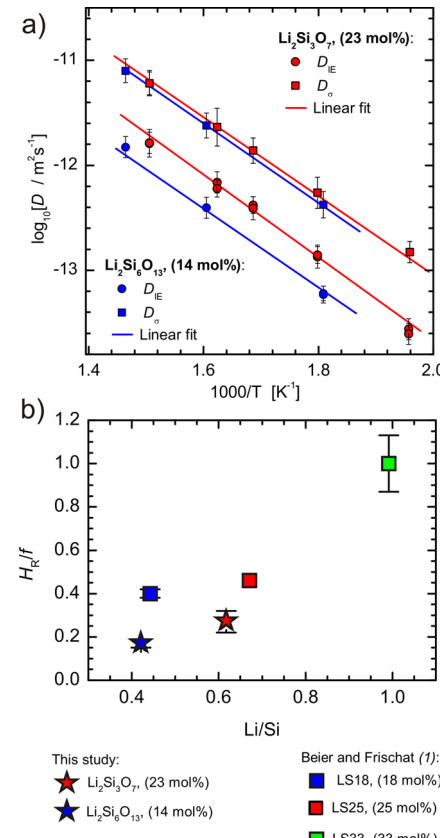


**Figure 10.** (a) Comparison of lithium diffusivities determined by isotope exchange experiments and DC electrical conductivity for  $\text{Li}_2\text{Si}_3\text{O}_7$  and  $\text{Li}_2\text{Si}_6\text{O}_{13}$  glasses. (b) Average correlation factor  $H_R/f$  as a function of Li/Si content including data from Beier and Frischat.<sup>1,2</sup>

The valuable insight into the prevailing migration mechanism and the effectiveness of individual jumps can be obtained through the comparison of the tracer diffusion coefficient  $D_i^*$  and the ionic diffusivity,  $D_{i,\sigma}$

$$D_i^* = D_{i,\sigma} H_R \quad (7)$$

in which  $D_{i,\sigma}$  corresponds to the diffusion coefficient derived from ionic conductivity.<sup>2,62,63</sup> The Haven ratio  $H_R$  is a correction factor in the Nernst–Einstein relation (eq 5) caused by the correlated charge transport, which results directly in a decrease of the diffusion coefficient. When  $H_R = 1$ , an individual independent charge transport can be assumed. Since no tracer isotope is available for lithium and self-diffusion coefficients  $D_{i,IE}$  are measured by isotope exchange experiments, eq 7 has to be modified taking into account that the self-diffusion coefficient is proportional to  $D_i^*$

$$D_i^* = f D_{i,IE} \quad (8)$$

The correlation factor  $f$  can vary between 0 and 1 depending on the diffusion mechanism.

Combining eqs 7 and 8, the  $H_R/f$  ratio links the self-diffusion with the ionic diffusivity

$$D_{i,IE} = \frac{H_R}{f} D_{i,\sigma} \quad (9)$$

In single-crystal materials, a low  $H_R/f$  value indicates a vacancy-dominated and significantly correlated movement, whereas  $H_R/f = 1$  points to uncorrelated jumps via interstitials.<sup>62</sup> In the case of glasses where long-range periodicity is absent, interpretation of correlation effects is not as straightforward. To overcome that problem, Wegener and Frischat<sup>64</sup> proposed a model in which the glass network is treated as consisting of many randomly oriented crystallites and the full long-range motion is observed as a sequence of numerous small steps. This allows transferring of ideas for the diffusion mechanism derived for crystals to glasses, although the definition of vacancies and interstitial sites is less clear for glasses.

The  $H_R/f$  values obtained for our glasses are listed in Table 3 together with literature data. The average  $H_R/f$  ratio decreases from  $0.27 \pm 0.05$  ( $1\sigma$ ) for the  $\text{Li}_2\text{Si}_3\text{O}_7$  glass to  $0.17 \pm 0.02$  ( $1\sigma$ ) for the  $\text{Li}_2\text{Si}_6\text{O}_{13}$  glass. High correlation of Li migration in both studied glasses can be well-explained in terms of percolation paths between Li-rich regions, impeded by low interconnectivity, low dimensionality, and high tortuosity. The correlation coefficients given by Beier and Frischat<sup>1,2</sup> corresponding to the  $D_{IE}/D_\sigma$  ratio vary between  $\sim 1$  for lithium-rich glasses, that is, LS33 ( $\approx \text{Li}_2\text{Si}_2\text{O}_5$ ), to  $\sim 0.4$  for lithium-poor LS18 ( $\approx \text{Li}_2\text{Si}_6\text{O}_{13}$ ) composition (see Figure 10b and Table 3). The decrease in  $H_R/f$  indicates a higher degree of Li transport correlation as a function of Li/Si ratio (Figure 10b). The change in transport properties appears to be particularly pronounced from  $\text{Li/Si} = 1.0$  to 0.7, that is, at the onset of phase separation in the glasses. That means that the formation of Li-poor regions embedded in a network of Li-rich low-dimensional interconnected areas induces strong correlation in long-range transport of lithium.

**5.5. Li Silicates versus Li Alumosilicates.** Introduction of aluminum into silicate glasses results in an increase of polymerization and, hence, in a fundamental change in the energy landscape in glass. When approaching  $\text{Li/Al} = 1$ , the network becomes completely polymerized. In the silicate, the negative charge is localized at the NBO, while in the polymerized alumosilicate, the charge is delocalized over the four BO bonds to Al cations. The energy minima created by NBOs in the silicate glasses are more localized than the minima created in the vicinity of  $[\text{AlO}_4]^-$  tetrahedra. According to the aluminum avoidance principle, that is, the “Loewenstein

rule”,<sup>65–67</sup> the building of Si–O–Al linkages is energetically favorable over the formation of pure Al–O–Al linkages. In this respect, the pronounced clustering of alkali ions as observed in binary silicate glasses is highly unlikely. The local potential on Li sites is determined by the distance and orientation to adjacent oxygens and by the fraction of Al in neighboring tetrahedra. MD simulations<sup>68</sup> have shown the lowest activation energy for Li diffusion in the case of the  $\text{LiAlSiO}_4$  system with alternating  $[\text{AlO}_4]^-$  and  $\text{SiO}_4$  tetrahedra and a uniform energy landscape. Increasing the  $\text{SiO}_2$  content at constant Li/Al (=1) results in an increase of activation energy, which can be explained by more pronounced local variations in the abundance of  $[\text{AlO}_4]^-$  units and, as a consequence, the variations in the local potential landscape.<sup>12</sup>

Consistent with this structural picture, lithium diffusion is about half of a log unit slower in lithium hexasilicate glass than that in  $\text{LiAlSi}_2\text{O}_6$  glass<sup>12</sup> (Figure 8). Both glasses have the same ratio of lithium to tetrahedral cations (1:3). The same experimental and analytical techniques were applied in both studies so that the data are directly comparable. The  $H_R/f$  value is significantly higher for the  $\text{LiAlSi}_2\text{O}_6$  ( $\sim 0.50^{12}$ ) than that for the  $\text{Li}_2\text{Si}_6\text{O}_{13}$  glass ( $\sim 0.17$ ), indicating that correlation of Li jumps is much more pronounced in the silicate glass at the same ratio of lithium to tetrahedral cations. In agreement with these observations, the  $E_{a,IE}$  for self-diffusion in  $\text{LiAlSi}_2\text{O}_6$  is slightly lower (67.1 kJ/mol) than that for the silicate (74.7 kJ/mol). Due to lower potential barriers, Li ions are more mobile in the aluminosilicate network, and long-range transport has higher efficiency. In Li silicate glasses, diffusion is facilitated in Li-rich regions by high abundance of suitable sites to host Li ions. On the other hand, long-range diffusion is limited by the dimensionality, tortuosity, and connectivity of Li-rich regions.

## 6. CONCLUSION

The characteristics of Li dynamics were determined for  $\text{Li}_2\text{Si}_3\text{O}_7$  and  $\text{Li}_2\text{Si}_6\text{O}_{13}$  glasses. Through comparison of our experimental results with those from the literature, it is apparent that for binary lithium silicate glasses with  $\text{Li}_2\text{O} \leq 33$  mol %, there is a strong influence of composition and nanoscale phase separation on Li mobility. This tendency for phase separation is reflected in local structural arrangement of depolymerized Q species, namely,  $Q^3$  and  $Q^2$ , as they characterize the Li-rich regions imbedded in an insulating Si rich matrix. Thermal treatments near or above  $T_g$  also significantly influence Li clustering<sup>1,2</sup> and, hence, the characteristics of Li-rich regions, namely, abundance, spatial distribution, interconnectivity, and volume coupled with cation density, shaping the percolation paths for the Li transport. The strong influence of those structural arrangements on percolation pathways are further exhibited in the rising degree of correlation in collective cation jumps, expressed as  $H_R/f$ , with decreasing Li concentration. An increasingly correlated Li migration coupled with increasing  $\text{SiO}_2$  content can be attributed to the enhanced constriction, elongation, and tortuosity of percolation paths used for Li migration.

## ■ AUTHOR INFORMATION

### Corresponding Authors

\*E-mail: u.bauer@mineralogie.uni-hannover.de. Tel.: +49 (0) 511 762-4818 (U.B.).

\*E-mail: a.m.welsch@mineralogie.uni-hannover.de (A.-M.W.).

**Notes**

The authors declare no competing financial interest.

**ACKNOWLEDGMENTS**

The authors are grateful for the financial support from DFG via FOR 1277. The help of Lars Dörrer, Sebastian Ross, Dawid Murawski, Marc Krey, and Eric Wolff was of particular importance and is greatly appreciated. We are thankful to Mareille Wittnebel for the preparation of diffusion couples and Otto Diedrich and Julian Feige for the preparation of excellent glass sections.

**REFERENCES**

- (1) Beier, W.; Frischat, G. H. Transport Mechanisms in Alkali Silicate Glasses. *J. Non-Cryst. Solids* **1985**, *73*, 113–133.
- (2) Beier, W.; Frischat, G. H. Lithium-Selbstdiffusion in Lithiumsilicatgläsern. *Glastech. Ber.* **1984**, *57*, 71–80.
- (3) Beier, W.; Frischat, G. H. A Mass Spectrometric Method for the Determination of Li Self Diffusion in Oxide Glasses. *J. Non-Cryst. Solids* **1980**, *38*, 569–573.
- (4) Haynes, W. M. CRC Handbook of Chemistry and Physics, 91st ed.; CRC Press, Inc.: Boca Raton, FL, 2010–2011.
- (5) Feinauer, A.; Majer, G.; Seeger, A. The Diffusion of  ${}^6\text{Li}$  and  ${}^7\text{Li}$  and the Isotope Effect in Liquid Lithium. *J. Phys.: Condens. Matter* **1994**, *6*, L355–L360.
- (6) Feinauer, A.; Majer, G.; Seeger, A. Self-Diffusion in Liquid Lithium and Sodium. *J. Defect Diff. Forum* **1997**, *881*, 143–147.
- (7) Omini, M. Self-Diffusion and Inter-Diffusion Coefficients of Liquid Lithium Isotopes. *Philos. Mag.* **2006**, *86*, 1643–1666.
- (8) Omini, M. Diffusion Process in a Liquid Mixture of Lithium Isotopes. *Philos. Mag.* **2009**, *89*, 1–25.
- (9) Horn, I.; von Blanckenburg, F.; Schoenberg, R.; Steinhofel, G.; Markl, G. In Situ Iron Isotope Ratio Determination Using UV-Femtosecond Laser Ablation with Application to Hydrothermal Ore Formation Processes. *Geochim. Cosmochim. Acta* **2006**, *70*, 3677–3688.
- (10) Horn, I.; von Blanckenburg, F. Investigation on Elemental and Isotopic Fractionation during 196 nm Femtosecond Laser Ablation Multiple Collector Inductively Coupled Plasma Mass Spectrometry. *Spectrochim. Acta, Part B* **2007**, *62*, 410–422.
- (11) Horn, I. Mineralogical Association of Canada Short Course 40, Mineralogical Association of Canada: Vancouver, B.C., 2008; pp 53–65.
- (12) Welsch, A.-M.; Behrens, H.; Horn, I.; Ross, S.; Heitjans, P. Self-Diffusion of Lithium in  $\text{LiAlSi}_2\text{O}_6$  Glasses Studied Using Mass Spectrometry. *J. Phys. Chem. A* **2012**, *116*, 309–318.
- (13) Voigt, U.; Lammert, H.; Eckert, H.; Heuer, A. Cation Clustering in Lithium Silicate Glasses: Quantitative Description by Solid-State NMR and Molecular Dynamics Simulations. *Phys. Rev. B* **2005**, *72*, 064207/1–064207/11.
- (14) Du, J.; Corrales, L. R. Structure, Dynamics, and Electronic Properties of Lithium Disilicate Melt and Glass. *J. Chem. Phys.* **2006**, *125*, 114702/1–114702/12.
- (15) Zhao, J.; Gaskell, P. H.; Cluckie, M. M.; Soper, A. K. A Neutron Diffraction, Isotopic Substitution Study of the Structure of  $\text{Li}_2\text{O}\cdot 2\text{SiO}_2$  Glass. *J. Non-Cryst. Solids* **1998**, *232–234*, 721–727.
- (16) Kargl, F.; Meyer, A.; Koza, M. M.; Schober, H. Formation of Channels for Fast-Ion Diffusion in Alkali Silicate Melts: A Quasielastic Neutron Scattering Study. *Phys. Rev. B* **2006**, *74*, 014304/1–014304/5.
- (17) Vogel, W. *Struktur und Kristallisation der Gläser*; VEB Deutscher Verlag für Grundstoffindustrie: Leipzig, Germany, 1971.
- (18) Greaves, G. N. EXAFS and the Structure of Glass. *J. Non-Cryst. Solids* **1985**, *71*, 203–217.
- (19) Greaves, G. N.; Ngai, K. L. Reconciling Ionic-Transport Properties with Atomic Structure in Oxide Glasses. *Phys. Rev. B* **1995**, *52*, 6358–6380.
- (20) Greaves, G. N.; Gurman, S. J.; Catlow, C. R. A.; Chadwick, A. V.; Houde-Walter, A.; Henderson, C. M. B.; Dobson, B. R. A Structural Basis for Ionic-Diffusion in Oxide Glasses. *Philos. Mag. A* **1991**, *64*, 1059–1072.
- (21) Lee, S. K.; Stebbins, J. F. Effects of the Degree of Polymerization on the Structure of Sodium Silicate and Aluminosilicate Glasses and Melts: An  ${}^{17}\text{O}$  NMR Study. *Geochim. Cosmochim. Acta* **2009**, *73*, 1109–1119.
- (22) Hench, L. L.; Frieman, S. W.; Kinser, D. L. The Early Stages of Crystallization in a  $\text{Li}_2\text{O}\cdot \text{SiO}_2$  Glass. *Phys. Chem. Glasses* **1971**, *12*, 58–63.
- (23) Kracek, F. C. The Binary System  $\text{Li}_2\text{O}\cdot \text{SiO}_2$ . *J. Phys. Chem.* **1930**, *34*, 2641–2650.
- (24) Migge, H. Estimation of Free Energies for  $\text{Li}_8\text{SiO}_6$  and  $\text{Li}_4\text{SiO}_4$  and Calculation of the Phase Diagram of the Li–Si–O System. *J. Nucl. Mater.* **1988**, *151*, 101–107.
- (25) Pochou, J. L.; Pichoir, F. *Electron Probe Quantitation*; Plenum Press Division Plenum Publishing Corp.: New York, 1991; pp 31–75.
- (26) HVG-DGG. <http://www.hvg-dgg.de/download/freie-inhalte/standardglas.html> (2013).
- (27) Rahn, J.; Huger, E.; Dorrer, L.; Ruprecht, B.; Heitjans, P.; Schmidt, H. Li Self-Diffusion in Lithium Niobate Single Crystals at Low Temperatures. *Phys. Chem. Chem. Phys.* **2012**, *14*, 2427–2433.
- (28) Blank, K. Elektrische Leitfähigkeit von Alkali Silicat Gläsern. *Glastech. Ber.* **1966**, *39*, 489–496.
- (29) Charles, R. J. Metastable Liquid Immiscibility in Alkali Metal Oxide-Silica Systems. *J. Am. Ceram. Soc.* **1966**, *49*, 55–62.
- (30) Crank, J. *the Mathematics of Diffusion*, 2nd ed.; Clarendon Press: London, 1975.
- (31) Koepcke, J.; Behrens, H. Trace Element Diffusion in Andesitic Melts: An Application of Synchrotron X-ray Fluorescence Analysis. *Geochim. Cosmochim. Acta* **2001**, *226*, 1481–1498.
- (32) Funke, K.; Banhatti, R. D.; Laughman, D. M.; Badr, L. G.; Mutke, M.; Šantić, A.; Wrobel, W.; Fellberg, E. M.; Biermann, C. First and Second Universalities: Expeditions Towards and Beyond. *Z. Phys. Chem.* **2010**, *224*, 1891–1950.
- (33) Ingram, M.; Imrie, C. T. New Insights from Variable-Temperature and Variable-Pressure Studies into Coupling and Decoupling Processes for Ion Transport in Polymer Electrolytes and Glasses. *Solid State Ionics* **2011**, *196*, 9–17.
- (34) Soltay, L. G.; Henderson, G. S. The Structure of Lithium-Containing Silicate and Germanate Glasses. *Can. Mineral.* **2005**, *43*, 1643–1651.
- (35) Mysen, B. O.; Richet, P. *Silicate Glasses and Melts: Properties and Structure; Developments in Geochemistry 10*; Elsevier: Amsterdam, The Netherlands, 2005.
- (36) Schramm, C. M.; deJong, B. H. W. S.; Parziale, V. E.  ${}^{29}\text{Si}$  Magic Angle Spinning NMR Study on Local Silicon Environments in Amorphous and Crystalline Lithium Silicates. *J. Am. Chem. Soc.* **1984**, *106*, 4396–4402.
- (37) Zakaznova-Herzog, V. P.; Malfait, W. J.; Herzog, F.; Halter, W. E. Quantitative Raman Spectroscopy: Principles and Application to Potassium Silicate Glasses. *J. Non-Cryst. Solids* **2007**, *353*, 4015–4028.
- (38) Herzog, F.; Zakaznova-Herzog, V. P. Quantitative Raman Spectroscopy: Challenges, Shortfalls, and Solutions—Application to Calcium Silicate Glasses. *Am. Mineral.* **2011**, *96*, 914–927.
- (39) Malfait, W. J.; Zakaznova-Herzog, V. P.; Halter, W. E. Quantitative Raman Spectroscopy: High-Temperature Speciation of Potassium Silicate Melts. *J. Non-Cryst. Solids* **2007**, *353*, 4029–4042.
- (40) Malfait, W. J.; Zakaznova-Herzog, V. P.; Halter, W. E. Amorphous Materials: Properties, Structure, and Durability: Quantitative Raman Spectroscopy: Speciation of Na-Silicate Glasses and Melts. *Am. Mineral.* **2008**, *93*, 1505–1518.
- (41) McMillan, P. F.; Wolf, G. H.; Poe, B. T. Vibrational Spectroscopy of Silicate Liquids and Glasses. *Chem. Geol.* **1992**, *96*, 351–366.
- (42) Mysen, B. O.; Frantz, J. D. Silicate Melts at Magmatic Temperatures — In-situ Structure Determination to 1651°C and

- Effect of Temperature and Bulk Composition on the Mixing Behavior of Structural Units. *Contrib. Mineral. Petrol.* **1994**, *117*, 1–14.
- (43) McMillan, P. F.; Wolf, G. H. Vibrational Spectroscopy of Silicate Liquids. *Rev. Min. Geochem.* **1995**, *32*, 247–315.
- (44) Larson, C.; Doerr, J.; Affigato, M.; Feller, S.; Holland, D.; Smith, M. E. A  $^{29}\text{Si}$  MAS NMR Study of Silicate Glasses with a High Lithium Content. *J. Phys.: Condens. Matter* **2006**, *18*, 11323–11331.
- (45) Dupree, R.; Holland, D.; Mortuza, M. G. A MAS-NMR Investigation of Lithium Silicate-Glasses and Glass-Ceramics. *J. Non-Cryst. Solids* **1990**, *116*, 148–160.
- (46) Maekawa, H.; Maekawa, T.; Kawamura, K.; Yokokawa, T. The Structural Groups of Alkali Silicate-Glasses Determined from  $^{29}\text{Si}$  MAS-NMR. *J. Non-Cryst. Solids* **1991**, *127*, 53–64.
- (47) Halter, W. E.; Mysen, B. O. Melt Speciation in the System  $\text{Na}_2\text{O}-\text{SiO}_2$ . *Chem. Geol.* **2004**, *213*, 115–123.
- (48) Nesbitt, H. W.; Bancroft, G. M.; Henderson, G. S.; Ho, R.; Dalby, K. N.; Huang, Y.; Yan, Z. Bridging, Non-bridging and Free ( $\text{O}^{2-}$ ) Oxygen in  $\text{Na}_2\text{O}-\text{SiO}_2$  Glasses: An X-ray Photoelectron Spectroscopic (XPS) and Nuclear Magnetic Resonance (NMR) Study. *J. Non-Cryst. Solids* **2011**, *357*, 170–180.
- (49) Sen, S.; Youngman, R. E. NMR Study of Q-Speciation and Connectivity in  $\text{K}_2\text{O}-\text{SiO}_2$  Glasses with High Silica Content. *J. Non-Cryst. Solids* **2003**, *331*, 100–107.
- (50) Shannon, R. D.; Prewitt, C. T. Effective Ionic Radii in Oxides and Fluorides. *Acta Crystallogr., Sect. B* **1969**, *25*, 925–946.
- (51) Kamijo, N.; Handa, K.; Umesaki, N. Soft X-ray XAFS Studies on the Local Structure of  $\text{K}_2\text{O}-\text{SiO}_2$  Glasses. *Mater. Trans., JIM* **1996**, *37*, 927–931.
- (52) Fabian, M.; Jovari, P.; Svab, E.; Meszaros, Gy.; Proffen, T.; Veress, E. Network Structure of 0.7 $\text{SiO}_2$ -0.3 $\text{Na}_2\text{O}$  Glass from Neutron and X-ray Diffraction and RMC Modelling. *J. Phys.: Condens. Matter* **2007**, *19*, 335209/1–335209/11.
- (53) Uhlig, H.; Hoffmann, M. J.; Lamparter, H.-P.; Aldringer, F.; Bellissent, R.; Steeb, S. Short-Range and Medium-Range Order in Lithium Silicate Glasses, Part I: Diffraction Experiments and Results. *J. Am. Ceram. Soc.* **1996**, *79*, 2833–2838.
- (54) Hannon, A. C.; Vessal, B.; Park, J. M. The Structure of Alkali Silicate-Glasses. *J. Non-Cryst. Solids* **1992**, *150*, 97–102.
- (55) Göbel, E.; Müller-Warmuth, W.; Olyschläger, H.; Dutz, H.  $^7\text{Li}$  NMR-Spectra, Nuclear-Relaxation, and Lithium Ion Motion in Alkali Silicate, Borate, and Phosphate-Glasses. *J. Magn. Reson.* **1979**, *36*, 371–387.
- (56) Kuhn, A.; Wilkening, M.; Heitjans, P. Mechanically Induced Decrease of the Li Conductivity in an Alumosilicate Glass. *Solid State Ionics* **2009**, *180*, 302–307.
- (57) Sen, S.; Mukerji, T. A Molecular Dynamics Simulation Study of Ionic Diffusion and NMR Spin-Lattice Relaxation in  $\text{Li}_2\text{Si}_4\text{O}_9$  Glass. *J. Non-Cryst. Solids* **2001**, *293–295*, 268–278.
- (58) Lammert, H.; Heuer, A. Emergence of Conduction Channels in Lithium Silicate. *Phys. Rev. B* **2004**, *70*, 024204/1–024204/5.
- (59) Habasaki, J.; Hiwatari, Y. Molecular Dynamics Study of the Mechanism of Ion Transport in Lithium Silicate Glasses: Characteristics of the Potential Energy Surface and Structures. *Phys. Rev. B* **2004**, *69*, 144207/1–144207/17.
- (60) Prasada Rao, R.; Tho, T. D.; Adams, S. Ion Transport Pathways in Molecular Dynamics Simulated Lithium Silicate Glasses. *Solid State Ionics* **2010**, *181*, 1–6.
- (61) Dullien, F. A. L. *Porous Media — Fluid Transport and Pore Structure*, 2nd ed.; Academic Press: San Diego, CA, 1992.
- (62) Mehrer, H. *Diffusion in Solids — Fundamentals, Methods, Materials, Diffusion-Controlled Processes*. Springer Ser. Solid-State Sci. **2007**, *155*.
- (63) Lonergan, M. C.; Shriver, D. F.; Ratner, M. A. Polymer Electrolytes — The Importance of Ion-Ion Interactions in Diffusion Dominated Behavior. *Electrochim. Acta* **1995**, *40*, 2041–2048.
- (64) Wegener, W.; Frischat, G. H. Calculation of Correlation Factors for Sodium Self Diffusion in Glassy Sodium Disilicate. *J. Non-Cryst. Solids* **1982**, *50*, 253–261.
- (65) Cormier, L.; Gaskell, P. H.; Calas, G.; Zhao, J.; Soper, A. K. Environment Around Li in the  $\text{LiAlSiO}_4$  Ionic Conductor Glass: A Neutron-Scattering and Reverse Monte Carlo Study. *Phys. Rev. B* **1998**, *57*, R8067–R8070.
- (66) Pechnik, A.; Whitmore, D. H.; Susman, S.; Ratner, M. A. Transport in Glassy Fast-Ion Conductors: A Study of  $\text{LiAlSiO}_4$  Glass. *J. Non-Cryst. Solids* **1988**, *101*, 54–64.
- (67) Loewenstein, W. The Distribution of Aluminium in the Tetrahedra of Silicates and Aluminates. *Am. Mineral.* **1954**, *39*, 92–96.
- (68) Li, W.; Garofalini, S. H. Molecular Dynamics Simulation of Lithium Diffusion in  $\text{Li}_2\text{O}-\text{Al}_2\text{O}_3-\text{SiO}_2$  Glasses. *Solid State Ionics* **2004**, *166*, 365–373.